The incoherent background

Assuming the Debye–Waller factor is a slowly varying function of Q, the counting rate due to the incoherent scattering is obtained from equations (10), (48) and (49):

$$I_{\text{inc}} = \frac{C_{\text{inc}}}{(Ma_1)^{1/2}} \left[\frac{v_2}{v_1 V(v_2+v_3)}\right]^{1/2} \tag{88}$$

where:

$$C_{\text{inc}} = \pi^2 \mathcal{V} \pi \Phi(\mathbf{k}_I)\varepsilon(k_I) N k_I^3 \frac{\mathrm{d}\sigma_{\text{inc}}}{\mathrm{d}\Omega} \frac{P_M}{|\mathrm{tg}\,\theta_M|}. \tag{89}$$

References

CAGLIOTI, G., PAOLETTI, A. & RICCI, F. P. (1958). *Nucl. Instrum. Meth.* **3**, 223–228.

CAGLIOTI, G., PAOLETTI, A. & RICCI, F. P. (1960). *Nucl. Instrum. Meth.* **9**, 195–198.

CAGLIOTTI, G. & RICCI, F. P. (1962). *Nucl. Instrum. Meth.* **15**, 155–163.

CASSELS, J. M. (1950). *Progr. Nucl. Phys.* **1**, 185–215.

COOPER, M. J. (1968). *Acta Cryst.* A**24**, 624–627.

COOPER, M. J. & NATHANS, R. (1967). *Acta Cryst.* **23**, 357–367.

COOPER, M. J. & NATHANS, R. (1968*a*). *Acta Cryst.* A**24**, 481–484.

COOPER, M. J. & NATHANS, R. (1968*b*). *Acta Cryst.* A**24**, 619–624.

GRABCEV, B. (1973*a*). Report IFA-FN-43, Institute for Atomic Physics, Bucharest.

GRABCEV, B. (1973*b*). *Nucl. Instrum. Meth.* **106**, 349–355.

SAILOR, V. L., FOOTE, H. L. JR, LANDON, H. H. & WOOD, R. E. (1956). *Rev. Sci. Instrum.* **27**, 26–34.

TEUTSCH, H. (1971). *Stud. Cerc. Fiz.* **23**, 517–553.

TUCCIARONE, A., LAU, H. Y., CORLISS, L. M., DELAPALME, A. & HASTINGS, J. M. (1971). *Phys. Rev.* B**4**, 3206–3245.

WILLIS, B. T. M. (1960). *Acta Cryst.* **13**, 763–766.

Acta Cryst. (1974). A**30**, 216

Interpretation of Short-Range-Order Scattering of Electrons; Application to Ordering of Defects in Vanadium Monoxide

BY B. ANDERSSON, J. GJØNNES AND J. TAFTØ

Department of Physics, University of Oslo, Oslo, Norway

(*Received* 16 *July* 1973; *accepted* 19 *September* 1973)

Diffuse scattering of electrons from local order of defects in vanadium monoxide of composition $VO_{1.23}$ has been studied above the ordering temperature. Intensity expressions for short-range-order scattering involving defects of more than one kind are derived, both for the kinematical case and with Bragg scattering effects included. The interpretation is based upon comparison between experimental and calculated distributions in intensity space and vector space, mainly in projections where Bragg scattering effects are small or moderate. The scattering can be interpreted in terms of defect clusters consisting of one metal interstitial surrounded by four metal vacancies, as in the ordered structure $V_{52}O_{64}$. The local arrangement of clusters is different from that found in the ordered phase, however.

1. Introduction

The ease with which patterns of diffuse scattering from single crystals can be obtained in electron diffraction has made it a useful tool for the study of local order of defects. However, emphasis in applications has almost exclusively been on the qualitative side. Quantitative interpretation of diffuse scattering in terms of order parameters, as was developed in the X-ray case some 20 years ago, has been tried only to a very limited extent. The main reasons for this are associated with the strong interaction between the incident electron and the crystal. This may call for more complicated intensity expressions than those given by kinematical theory, especially when strong Bragg reflexions are excited, and will also render the extraction of short-range-order scattering from other types of diffuse scattering more difficult.

General expressions for diffuse scattering of electrons including dynamical interactions through Bragg reflexions have previously been developed (Gjønnes, 1965, 1966; Gjønnes & Höier, 1971). It was found that substitutional short-range order in binary alloys represents a relatively simple case (Fisher, 1965), the Bragg scattering effects leading mainly to a redistribution of diffuse scattering between different Brillouin zones. When more than one lattice site is involved in the ordering, the situation becomes more complicated, but also more interesting, since the Bragg scattering effects on the diffuse scattering may then introduce features which carry information which is not contained in purely kinematical experiments.

Our reasons for starting a study on the vanadium–oxygen system stemmed, to some extent, from such considerations. The defect rocksalt-type oxides of transition metals (TiO, FeO, VO, *etc.*) contain many de-

fects, frequently vacancies on both the metal and the oxygen lattices and sometimes also metal interstitials. A further reason for using electron diffraction is, of course, that X-ray diffraction is difficult to apply because of lack of suitable single crystals.

A description of the various types of diffuse scattering in the monoxide region, which extends from $x \simeq 0{\cdot}85$ to 1·23 at 800 °C (Westman & Nordmark, 1960) and of their relation to the ordered, low-temperature structures present will be given elsewhere. In the present paper we shall be concerned with diffuse scattering at the composition $VO_{1\cdot23}$ from samples annealed at 850 °C, that is 50 °C above the transition temperature of the ordered phase $V_{52}O_{64}$ (Andersson & Gjønnes, 1970). This phase can be described as an ordered arrangement of defect clusters consisting of one metal interstitial at a tetrahedral position, surrounded by four metal vacancies. The resulting tetragonal structure shows only slight tetragonal distortion of the fundamental cubic cell. Patterns of diffuse scattering taken at 1 MV (Andersson, Gjønnes & Taftø, 1971) indicate that the diffuse scattering can be separated into an outer region where atomic displacements or 'size effects' are important and an inner part where the substitutional-order scattering is predominant.

The aim of the present work is to present and discuss methods for quantitative interpretation of short-range-order diffuse scattering and to apply them to scattering from disordered $VO_{1\cdot23}$. The scattering is, so far, assumed to be connected with substitutional order; effects due to static displacements and thermal motion have thus been neglected. The theory and calculation methods have been developed to include dynamical effects, but at the present stage emphasis has been put on application of kinematical expressions as far as these can be carried. We have also, to a certain extent, relied upon our knowledge of the ordered, low-temperature structure, particularly the existence of tetrahedral defect clusters. Measurements of the 200 structure factor for disordered $VO_{1\cdot23}$ (Høier & Andersson, 1974) has recently produced supporting evidence for the existence of these also above the ordering temperature.

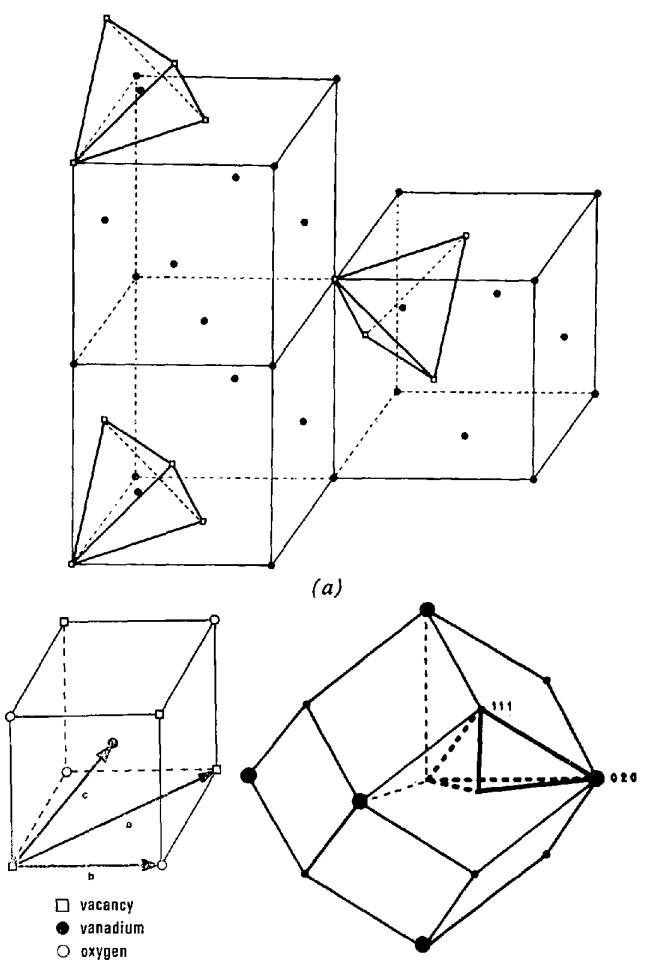

Fig. 1. (*a*) Part of the ordered structure $V_{52}O_{64}$ including the three shortest intercluster vectors. The oxygen atoms are not shown. (*b*) Tetrahedral cluster with the shortest vectors of the types **a**, **b** and **c**. (*c*) The Brillouin zone for diffuse scattering.

2. Theory

(*a*) *Kinematical scattering, order parameters*

The theory for scattering from substitutional short-range order has mainly been developed for binary alloys where ordering takes place only on one lattice site. The V–O system includes, in general, occupied and vacant sites both on the f.c.c. metal and oxygen sublattices and, in addition, metal interstitials on the two f.c.c. sublattices formed by the tetrahedral interstitial positions, $\pm(\frac{1}{4}\frac{1}{4}\frac{1}{4})$, see Fig. 1(*a*,*b*).

The extension of the usual theory (Warren, Averbach & Roberts, 1951; Cowley, 1950) to such more complex systems is fairly straightforward, see *e.g.* Elcock (1956). Let $\beta_{Mj},\beta_{tj},\beta_{oj}$ be occupation numbers on the normal metal, interstitial and oxygen sublattices. The amplitude of scattering can be written as a sum of three terms:

$$F(\mathbf{s})\sum_{1}^{N}\beta_{Mj}f_M\exp\left[-i\mathbf{s}\,.\,\mathbf{r}_{Mj}\right]+\sum_{1}^{2N}\beta_{tj}f_M\exp\left[-i\mathbf{s}\,.\,\mathbf{r}_{tj}\right]+\sum_{1}^{N}\beta_{oj}f_o\exp\left[-i\,.\,\mathbf{r}\mathbf{s}_{oj}\right] \quad (1)$$

where N is the number of positions on each lattice, f_M and f_o are scattering factors for vanadium and oxygen, $\mathbf{r}_{oj}$ *etc.* are lattice positions.* The scattered intensity is made up of nine terms:

$$I_1(\mathbf{s})=\sum\sum\beta_{Mj}\beta_{Mj'}f_M^2\exp\left[-i\mathbf{s}(\mathbf{r}_{Mj}-\mathbf{r}_{Mj'})\right]$$

$$I_2(\mathbf{s})=\sum\sum\beta_{Mj}\beta_{tj'}f_M^2\exp\left[-i\mathbf{s}(\mathbf{r}_{Mj}-\mathbf{r}_{tj'})\right]$$

etc.

* M is used as subscript for vanadium throughout to avoid confusion with vacancies.

The sums over products of two occupation numbers can be written in terms of probabilities, P_{MMj} *etc.* associated with vectors $\mathbf{a}_j$ *etc.* in Patterson space.

$$\begin{aligned} I_1 &= Nf_M^2 c_M \sum_j P_{MMj} \exp[-i\mathbf{s}\cdot\mathbf{a}_j] \\ I_2 &= Nf_M^2 c_M \sum_j P_{Mtj} \exp[-i\mathbf{s}\cdot\mathbf{c}_j] \\ I_4 &= 2Nf_M^2 c_t \sum_j P_{tMj} \exp[-i\mathbf{s}\cdot\mathbf{c}_j] \\ I_5 &= 2Nf_M^2 c_t\{\sum_j P_{ttj}^{(1)} \exp[-i\mathbf{s}\cdot\mathbf{a}_j] \\ &\quad + \sum_j P_{ttj}^{(2)} \exp[-i\mathbf{s}\cdot\mathbf{b}_j]\} \quad (2) \end{aligned}$$

for the terms which are left when the oxygen lattice is assumed to be perfect and therefore disregarded in the derivation of diffuse scattering. In equation (2) c_M and c_t are average occupation numbers. The vectors $\mathbf{a}_j$ connect two positions on the same sublattice, *i.e.* two octahedral sites or two tetrahedral sites belonging to the same f.c.c. lattice, whereas the vectors $\mathbf{c}_j$ connect octahedral and tetrahedral positions and $\mathbf{b}_j$ connect positions on the two sets of tetrahedral positions. The probabilities P_{MMj} P_{Mtj}, P_{tMj}, $P_{ttj}^{(1)}$ and $P_{tjj}^{(2)}$ are associated with metal–metal, metal–interstitial, interstitial–metal and interstitial–interstitial pairs; the last being of two types depending upon whether the two interstitials are positioned on the same or on different sublattices, see Fig. 1(*b*).

For $|\mathbf{a}_j|$, $|\mathbf{c}_j|$ and $|\mathbf{b}_j| \to \infty$

$$P_{MMj}, P_{tMj} \to c_M \quad \text{and} \quad P_{Mtj}, P_{ttj} \to c_t .$$

On introducing the order parameters $\alpha_{MMj}=(p_{MMj}-c_M)/c_M$, $\alpha_{Mtj}=(P_{Mtj}-c_t)/c_t$ *etc.* we can separate out the short-range-order scattering parts:

$$\begin{aligned} I_{D1} &= Nf_M^2 c_M^2 \sum \alpha_{MMj} \exp[-i\mathbf{s}\cdot\mathbf{a}_j] \\ I_{D2} &= Nf_M^2 c_M c_t \sum \alpha_{Mtj} \exp[-i\mathbf{s}\cdot\mathbf{c}_j] \\ I_{D4} &= 2Nf_M^2 c_t c_M \sum \alpha_{tMj} \exp[-i\mathbf{s}\cdot\mathbf{c}_j] = I_{D2} \\ I_{D5} &= 2Nf_M^2 c_t^2\{\sum \alpha_{ttj}^{(1)} \exp[-i\mathbf{s}\cdot\mathbf{a}_j] \\ &\quad + \sum \alpha_{ttj}^{(2)} \exp[-i\mathbf{s}\cdot\mathbf{b}_j]\} . \quad (3a) \end{aligned}$$

The scattering expressions can be written in terms of order parameters for vacancies and interstitials. Completely analogous expressions to (3*a*) are obtained:

$$\begin{aligned} I_{D1} &= Nf_M^2 c_v^2 \sum \alpha_{vvj} \exp[-i\mathbf{s}\cdot\mathbf{a}_j] \\ I_{D2} &= -Nf_M^2 c_v c_t \sum \alpha_{vtj} \exp[-i\mathbf{s}\cdot\mathbf{c}_j] = I_{D4} \\ I_{D5} &= 2Nf_M^2 c_t^2\{\sum \alpha_{ttj}^{(2)} \exp[-i\mathbf{s}\cdot\mathbf{a}_j] \\ &\quad + \sum \alpha_{ttj}^{(2)} \exp[-i\mathbf{s}\cdot\mathbf{b}_j]\} \quad (3b) \end{aligned}$$

where α_{vvj}, α_{vtj} *etc.* are order parameters for vacancy–vacancy pairs, vacancy–interstitial pairs *etc.* $c_v=1-c_M$ is the average occupation number for vacancies at octahedral metal site. Note the change in sign for $I_{D2}=I_{D4}$.

When the three terms in equation (3*b*) are re-arranged according to the three sets of Patterson vectors $\mathbf{a}_j$, $\mathbf{b}_j$ and $\mathbf{c}_j$, the following expression for the total diffuse scattering is obtained:

$$\begin{aligned} I_D = Nf_M^2\{&\sum (c_v^2\alpha_{vvj} + 2c_t^2\alpha_{ttj}^{(1)} \exp[-i\mathbf{s}\cdot\mathbf{a}_j] \\ &- 2c_v c_t \sum \alpha_{vtj} \exp[-i\mathbf{s}\cdot\mathbf{c}_j] \\ &+ 2c_t^2 \sum \alpha_{ttj}^{(2)} \exp[-i\mathbf{s}\cdot\mathbf{b}_j]\} \quad (4) \end{aligned}$$

in which there are, essentially, four sets of order parameters; of these $\alpha_{tt}^{(2)}$, the α_{vt} and the combination $c_v^2\alpha_{vv}+c_t^2\alpha_{tt}^{(1)}$ can be determined from scattering experiments under kinematical conditions, assuming the average vacancy and interstitial occupation number to be known. The three sets of Patterson vectors define the Brillouin zone for the diffuse scattering, with zone boundaries as shown in Fig. 1(*c*).

(*b*) *Dynamical scattering*

Intensity expressions which include the effects of dynamical Bragg scattering on the distribution of diffuse scattering have been derived by many authors. The expression

$$\begin{aligned} I(\mathbf{s}+\mathbf{h}) = &\sum_g \sum_{g'} \sum_f \sum_{f'} \int_0^z S_{hg}(2) S_{hg'}^*(2) \\ &\times \langle F(\mathbf{s}+\mathbf{g}-\mathbf{f}) F^*(\mathbf{s}+\mathbf{g}'-\mathbf{f}')\rangle S_{f0}(1) S_{f'0}^*(1) \mathrm{d}z \quad (5) \end{aligned}$$

is due to Gjønnes (1966), where details are given. Bragg scattering of the incident beam and between diffuse beams is taken into account through the scattering matrix elements $S_{f0}(1)$ *etc.* and $S_{hg}(2)$ respectively. Here the abbreviated arguments (1) and (2) refer to the appropriate diffraction condition and thickness; $\mathbf{g},\mathbf{h},\mathbf{f}$ are reciprocal-lattice vectors, usually within a planar section of reciprocal space. The non-periodic part of the object, *i.e.* the sources of diffuse scattering, enters through the scattering function $\langle F(\mathbf{s}+\mathbf{g}-\mathbf{f})F^*(\mathbf{s}+\mathbf{g}'-\mathbf{f}')\rangle$ where $\mathbf{s}$ is a vector within the first Brillouin zone of the projection studied. Calculation of the intensity distribution in any particular case should be carried out using an expression like (5); however, a qualitative discussion of the effects to be expected can be based on the scattering function

$$Q(\mathbf{s},\mathbf{h}) = \langle F(s)^* F(\mathbf{s}+\mathbf{h})\rangle$$

where the restriction on $\mathbf{s}$ to lie within the first Brillouin zone is removed. $Q(\mathbf{s},\mathbf{h})$ can be expressed as a Fourier transform of $R(\mathbf{r},\mathbf{q})$ where $\mathbf{r}$ is a Patterson vector and $\mathbf{q}$ is a position within the fundamental cell defined by the Bragg reflexions (Gjønnes & Høier, 1971). In the present case of diffuse scattering from substitutional short-range order, R can be expressed in terms of order parameters for vacancy–vacancy, vacancy–interstitial and interstitial–interstitial pairs. It is then understood that only the amplitude parts which are associated with diffuse scattering should be included. Since we are dealing with static disorder, the brackets denoting the

average can be dropped. We shall now introduce these order parameters in the scattering function by starting with the amplitude expression, neglecting contributions from the oxygen,

$$F(\mathbf{s}+\mathbf{h})=\sum_1^N f_M\beta_{vj}\exp\left[-i(\mathbf{s}+\mathbf{h})\mathbf{r}_{vj}\right] + \sum_1^{2N} f_M\beta_{tj}\exp\left[-i(\mathbf{s}+\mathbf{h})r_{tj}\right]. \quad (6)$$

Expressions for the scattering function for different values of $\mathbf{h}$ can now be written down. We note that the h dependence is governed by phase factors of the type $\exp[i\mathbf{h}\,.\,\mathbf{r}_{vj}]$ and $\exp[i\mathbf{h}\,.\,\mathbf{r}_{tj}]$. The former is unity for all values of $\mathbf{h}$, whereas the tetrahedral positions will contribute different factors for reflexions of the types

$$A(h+k+l=4n);\ B(h+k+l=4n+2)$$

and

$$C(h+k+l=4n+1).$$

On proceeding from (6) in the same manner as with the kinematical expressions we obtain for reflexions of *type A*:

$$F(\mathbf{s})F^*(\mathbf{s}+\mathbf{h})=|F(\mathbf{s})|^2\,.\,f_M(|\mathbf{s}+\mathbf{h}|)/f(s) \quad (7a)$$

which differ from the direct, $|F(\mathbf{s})|^2$-term, only through the atomic scattering factor. For the other reflexions, the interstitial positions will contribute factors $\exp[i\mathbf{h}\,.\,\mathbf{r}_{tj}]\neq 1$ in the v–t and t–t pairs.

For reflexions of *type B* this factor is *minus* one, whence the contributions from v–t pairs will cancel together with the t–v pairs, since these will occur with the same probability.

The t–t pairs will all enter with a negative sign, hence

$$Q(\mathbf{s},\mathbf{h})=Nf_M(s)f_M(\mathbf{s}+\mathbf{h})\{\sum(c_v^2\alpha_{vvj}-2c_t^2\alpha_{ttj}^{(1)} \times\exp[-i\mathbf{s}\,.\,\mathbf{a}_j]-2c_t^2\sum\alpha_{ttj}^{(2)}\exp[-i\mathbf{s}\,.\,\mathbf{b}_j]\} \quad (7b)$$

where cosines may be substituted for the exponentials.

For reflexions of the *type C*, the v–v pairs are unchanged as before, whereas the v–t and t–v pairs can be calculated together from

$$f_M(s)f_M(\mathbf{s}+\mathbf{h})\sum\sum\beta_{vj}\beta_{tj'}\{\exp[-i\mathbf{s}\,.\,\mathbf{r}_{vj}] \times\exp[i(\mathbf{s}+\mathbf{h})\mathbf{r}_{tj'}]+\exp[-i\mathbf{s}\,.\,\mathbf{r}_{tj'}]\exp[i(\mathbf{s}+\mathbf{h})\mathbf{r}_{vj}]\} =f_M(s)f_M(\mathbf{s}+\mathbf{h})\sum\sum\beta_{vj}\beta_{tj'}\{\pm i\exp[i\mathbf{s}(\mathbf{r}_{vj}-\mathbf{r}_{tj'})] +\exp[i\mathbf{s}(\mathbf{r}_{vj}-\mathbf{r}_{tj'})]\},$$

where the upper sign within the braces refers to one set of tetrahedral positions, the lower sign to the other set. Adding the two, we obtain for the v–t and t–v pairs

$$f_M(s)f_M(\mathbf{s}+\mathbf{h})\sum\sum\beta_{vj}\beta_{tj'}\{2\sin[\mathbf{s}(\mathbf{r}_{vj}-\mathbf{r}_{tj'})] +2\cos[\mathbf{s}(\mathbf{r}_{vj}-\mathbf{r}_{tj'})]\}.$$

For the t–t pairs we get a sine contribution for pairs within the same set of tetrahedral positions (vectors $\mathbf{a}_j$). The vectors between the two sets give two contributions of opposite sign, which thence cancel. Thus:

$$Q(\mathbf{s},\mathbf{h})=Nf_M(s)f_M(\mathbf{s}+\mathbf{h})\{\sum c_v^2\alpha_{vvj}\cos(\mathbf{s}\,.\,\mathbf{a}_j) +c_t^2\alpha_{ttj}^{(1)}\sin(\mathbf{s}\,.\,\mathbf{a}_j)+\sum c_v\alpha_{vtj}[\cos(\mathbf{s}\,.\,\mathbf{c}_j) +\sin(\mathbf{s}\,.\,\mathbf{c}_j)]\}. \quad (7c)$$

(c) Scattering from clusters

The defect clusters can have two orientations [see Fig. 1(*a*)], according to whether the interstitial atom sits in one or the other of the two sets, $\mathbf{r}_t^{(1)}$ or $\mathbf{r}_t^{(2)}$, of tetrahedral positions. The scattering amplitudes for the two orientations of the cluster are

$$F_c(\mathbf{s})=f_M\{1-\sum_1^4\exp[-i\mathbf{s}\,.\,\mathbf{r}_{vj}]\}\text{ and }F_c^*(\mathbf{s}),$$

so that the amplitude for the assembly of clusters can be written:

$$F=\sum_t\beta_c^{(1)}\exp[-i\mathbf{s}\,.\,\mathbf{r}_t^{(1)}]F_c +\sum_t\beta_c^{(2)}\exp[-i\mathbf{s}\,.\,\mathbf{r}_t^{(2)}]F_c^*$$

from which we obtain an intensity expression in terms of probabilities P_{cc} associated with intercluster vectors $\mathbf{a}_j$ and $\mathbf{b}_j$ between clusters of the same or opposite types:

$$\begin{aligned}I&=\sum(c_cP_{ccj}^{(1)}+c_cP_{ccj}^{(2)})|F_c|^2\exp[-i\mathbf{s}\,.\,\mathbf{a}_j]\\&+\sum c_cP_{ccj}^{(1,2)}F_c^2\exp[-i\mathbf{s}\,.\,\mathbf{b}_j^{(1)}]\\&+c_cP_{cc}^{(2,1)}|F_c^*|^2\exp[-i\mathbf{s}\,.\,\mathbf{b}_j^{(2)}]\\&=2\sum c_cP_{cc}(\mathbf{a}_j)|F_c|^2\cos(\mathbf{s}\,.\,\mathbf{a}_j)\\&+2\sum c_cP_{cc}(\mathbf{b}_j)\,\mathrm{Re}\,\{F_c^2\exp[-i\mathbf{s}\,.\,\mathbf{b}_j]\}\end{aligned} \quad (8)$$

(the last sum is taken over one set, since we can arrange $\mathbf{b}_j^{(1)}=-\mathbf{b}_j^{(2)}$). In order to include Bragg scattering effects, we note that

$$F_c(\mathbf{s}+\mathbf{h})=f_M(\mathbf{s}+\mathbf{h})\{1-\sum_1^4\exp[-i\mathbf{s}\,.\,\mathbf{r}_j]\} \quad \text{for } h+k+l=4n$$

$$F_c(\mathbf{s}+\mathbf{h})=f_M(\mathbf{s}+\mathbf{h})\{1+\sum\exp[-i\mathbf{s}\,.\,\mathbf{r}_j]\} \quad \text{for } h+k+l=4n+2$$

$$F_c(\mathbf{s}+\mathbf{h})=f_M(\mathbf{s}+\mathbf{h})\{1\pm i\sum\exp[-i\mathbf{s}\,.\,\mathbf{r}_j]\} \quad \text{for } h+k+l=4n\pm1$$

and thus

(*A*) $F_c(\mathbf{s})F_c^*(\mathbf{s}+\mathbf{h})$: as $|F_c(s)|^2$ (apart from atomic scattering factor) for $h+k+l=4n$

(*B*) $: f_M(\mathbf{s}+\mathbf{h})f_M(\mathbf{s})\{1-\sum\}\{1+\sum^*\}$ for $h+k+l=4n+2$

(*C*) $: f_M(\mathbf{s}+\mathbf{h})f_M(\mathbf{s})\{1-\sum\}\{1\mp\sum^*\}$ for $h+k+l=4n\pm1$.

The above expressions can be used, together with the appropriate Bragg scattering factors $S_{hg}(2)$, $S_{f0}(1)$ *etc.* in equation (5), to obtain expressions for the distribution of diffuse scattering. They also serve as a very useful guide to conditions in which the Bragg scattering effects can be minimized. When the excited reflexions in the present case belong to the type $h+k+l=4n$, these effects will only consist of redistribution of scattering between different Brillouin zones, and in such a way that contributions from the different vectors are affected in exactly the same way. The most important of these effects may be Kikuchi lines and bands, these are usually weakest when the incident beam is near a zone axis. The errors involved on using a kinematical expression may therefore be avoided to some extent by choosing the incident beam along zone axes of the type ⟨111⟩, ⟨311⟩, *etc.*

Experimental

Vanadium metal (Koch-Light, 99·9%) and V_2O_3 (K & K 99·5%) were weighed out and arc-melted together in an argon atmosphere to produce specimens of composition $VO_{1.23}$. The samples, resting on a watercooled base, were rapidly quenched to room temperature. The specimens were heat-treated at 850°C for 3 weeks.

Oxidation to V_2O_5 of the samples in pure oxygen at 1 atm at 600°C for 48 h in order to check the composition, showed only small variations from the predetermined composition.

Specimens for examination in the electron microscope were prepared by metallographic polishing to approximately 0·5 mm thickness followed by electropolishing at a voltage of 13 V in an electrolyte containing 10% perchloric acid and 90% methanol at room temperature.

Selected area diffraction patterns were taken in a Philips EM 300 equipped with goniometer stage.

The diffuse scattering on the photographic plates was measured by means of a Joyce–Loebl photometer and the intensity data were recorded on magnetic tape.

The main features of the diffuse scattering, see Figs. 2 and 3, are maxima at $\frac{111}{222}$, $\frac{311}{222}$ *etc.*, which are connected through weak bridges in ⟨100⟩ directions. The maxima have a complex shape which differs somewhat from one equivalent position to another. Of the maxima those around {200} are particularly strong. Outside the maxima and bridges only very faint diffuse scattering is observed.

Calculations

The quantitative comparison between experimental and calculated scattering distributions calls for separation of the short-range-order scattering from a background of other types of diffuse scattering. The main contribution to this background will be inelastic scattering, which is strongly peaked about the central beam and also around other strong spots. Further, there will be thermal scattering and scattering from static displacements, which may contain features similar to the s.r.o. scattering. In addition, dynamical effects due to Bragg scattering may modify the s.r.o. scattering and also produce scattering effects like Kikuchi lines and bands in the continuous background. There will also, at any realistic thickness, be appreciable multiple diffuse scattering, the main effect of which will be to reduce the slope of the intensity curve. All these effects complicate the subtraction of a structure independent background. In contrast to the X-ray case no theoretical expression for the inelastic and thermal scattering can be given which permits subtraction of a theoretical background. The background was therefore drawn as a smooth, featureless curve, with no azimuthal variation (Fig. 4). Since our calculations, to a large extent, are based upon scattering from defect clusters, the background was drawn so that the structure-dependent part is everywhere positive. Scattering from independent clusters, and hence the Patterson peak at the origin, is thus included.

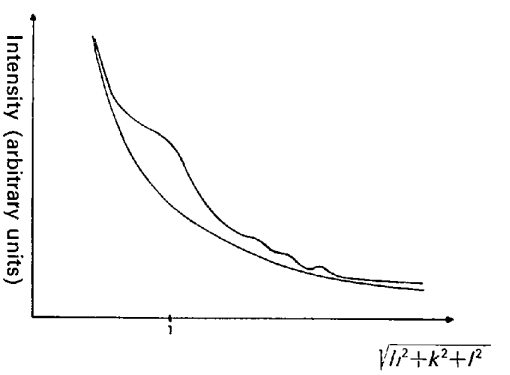

Fig. 4. Recorded intensity and drawn background along the [66$\bar{4}$] direction in the (311) projection.

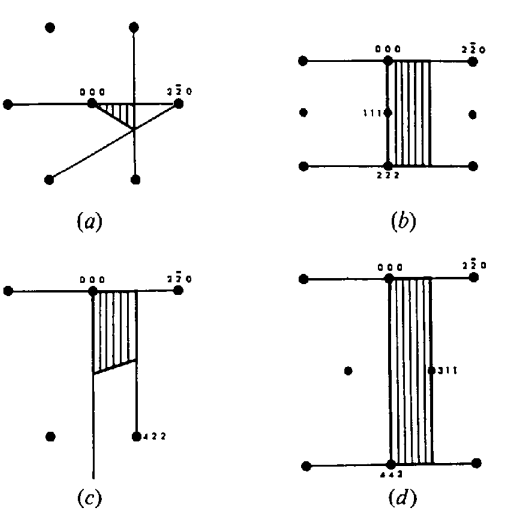

Fig. 5. Asymmetrical units in various planes in reciprocal space. (*a*) (11$\bar{1}$), (*b*) (11$\bar{2}$), (*c*) (11$\bar{3}$), (*d*) (11$\bar{4}$).

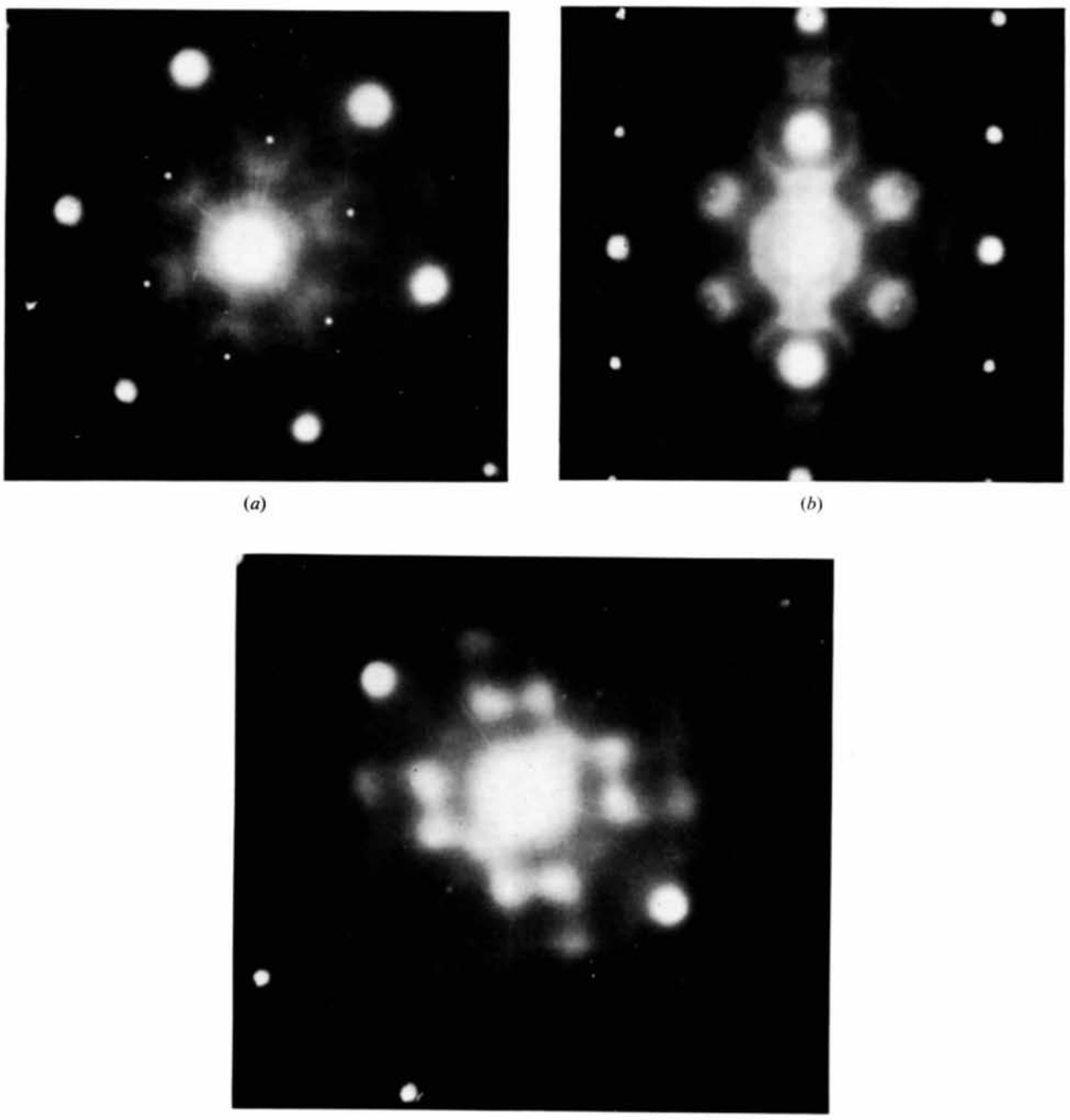

(*a*) (*b*)

(*c*)

Fig. 2. Diffraction from disordered $VO_{1\cdot23}$ heat-treated at 850 °C. 100 kV. (*a*) (111) projection; (*b*) (211) projection (*c*) (311) projection. Weak extra reflexions are due to presence of a nitride, $VN_{0\cdot35}$.

[*To face p.* 220

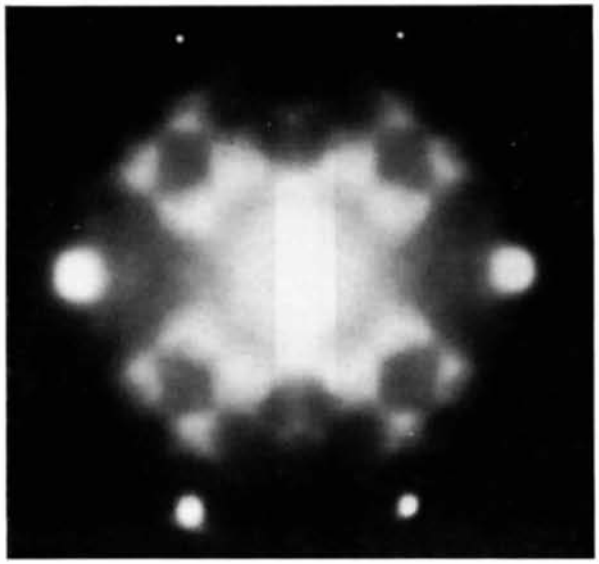

(*a*)

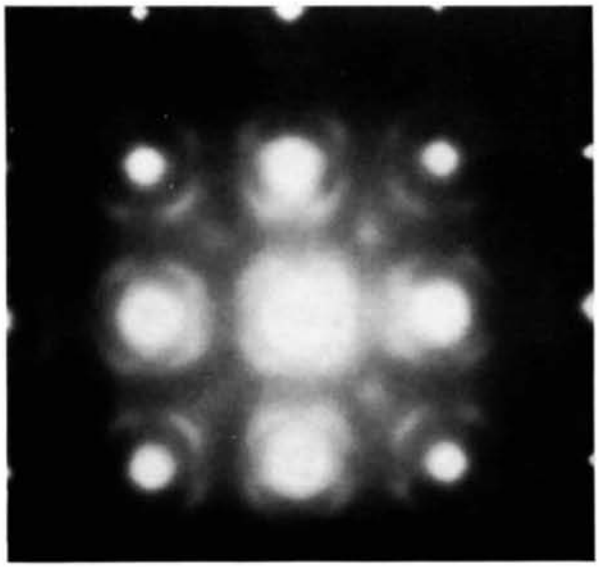

(*b*)

Fig. 3. Diffraction patterns from disordered $VO_{1.23}$ taken in the projections (*a*) (411), (*b*) (100).

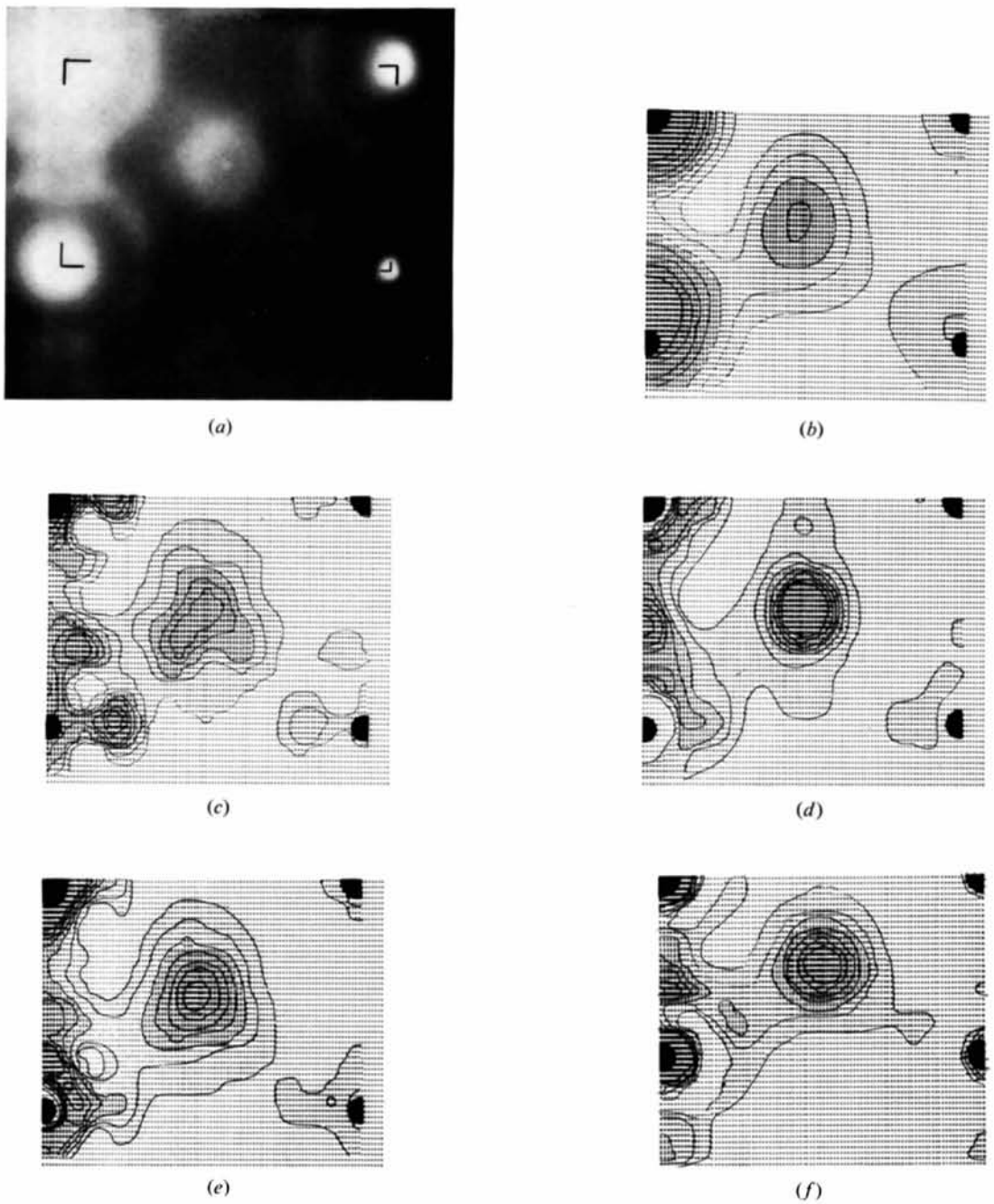

Fig. 6. Comparison between observed patterns of diffuse scattering in the (211) projection (*a*) and calculated distributions from: (*b*) isolated clusters, (*c*) small ordered domains of $V_{52}O_{64}$, (*d*) f.c.c. arrangement of clusters, (*e*) nearest-neighbour vectors $\langle 1\frac{1}{2}\frac{1}{2}\rangle$, $\langle 11\frac{1}{2}\rangle$ and $\langle 110\rangle$, (*f*) order parameters calculated from the (311) projection.

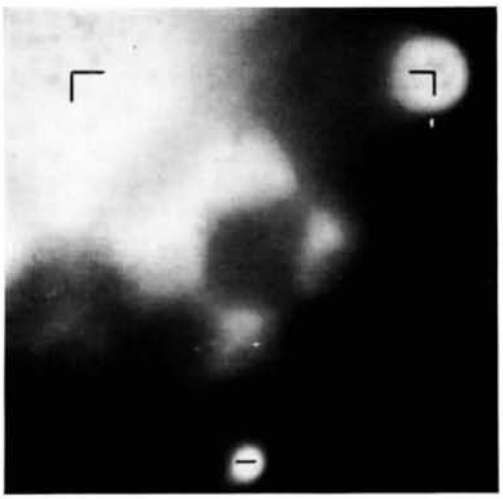

(*a*)

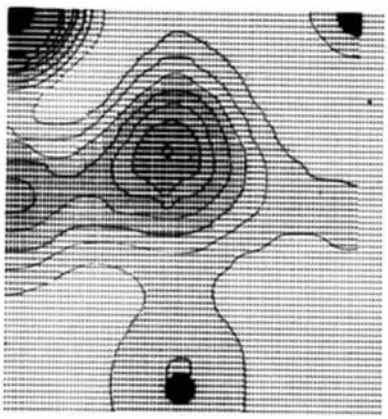

(*b*)

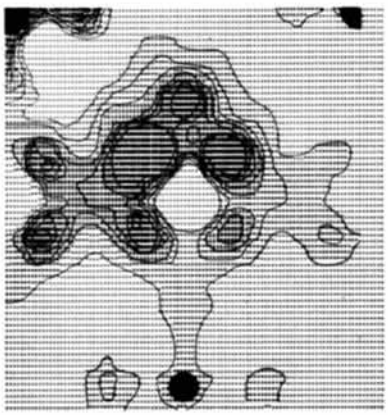

(*c*)

(*d*)

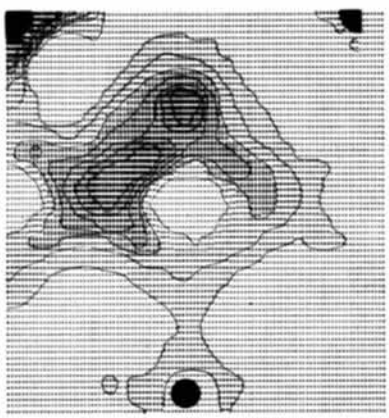

(*e*)

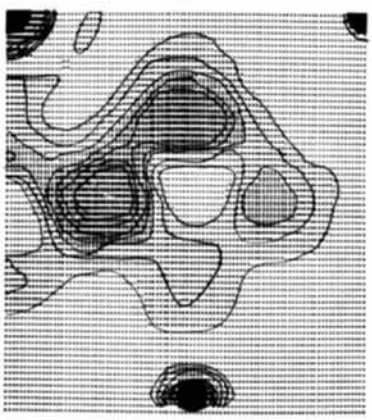

(*f*)

Fig. 7. Comparison between observed patterns of diffuse scattering in the (411) projection, (*a*) and calculated distributions from: (*b*) isolated clusters, (*c*) small ordered domains of $V_{52}O_{64}$, (*d*) f.c.c. arrangement of clusters, (*e*) nearest-neighbour vectors $\langle 1\frac{1}{2}\frac{1}{2}\rangle$, $\langle 11\frac{1}{2}\rangle$ and $\langle 110\rangle$, (*f*) order parameters calculated from the (311) projection.

Such a procedure implies, of course, that no corrections are applied for thermal scattering or for dynamical redistribution of the background intensity (Kikuchi lines and bands). However, the analysis was based mainly upon the intensity distribution within the inner Brillouin zone, where little contribution from thermal scattering and size effect is expected. Dynamical effects were kept low by using symmetrical incidence in projections with few Bragg spots, *viz.* [411] and [311].

Some attempts to use a three-dimensional intensity distribution were made, but the difficulties in constructing such a distribution from a series of patterns proved too formidable at the present stage.

The projections used correspond to rather long axes, hence to a dense vector net and a large unit in the section of reciprocal space (Fig. 5). As a consequence a fairly large amount of intensity data is used. It was hoped that this, to a certain extent, would mean increased information compared with the simpler projections.

The comparison with calculated intensity was performed by (*a*) trial-and-error methods, (*b*) partial Patterson syntheses, (*c*) least-squares calculations based on scattering from clusters.

(*a*) *Trial-and-error calculations*

Intensity calculations were carried out for several simple arrangements of tetrahedral clusters; some results are reproduced in Figs. 6 and 7 for isolated clusters (*b*); local order of clusters corresponding to small regions of the ordered phase (*c*); local order corresponding to an f.c.c. arrangement of clusters (*d*). Comparison with the observed patterns [Figs. 6(*a*), 7(*a*)], reveal distinct similarities between the calculated and experimental intensity distributions. In particular it appears that the groups of strong diffuse spots around the 200-type reflexions are related to local order involving the same type of defect clusters as are found in the ordered structure. However, the $V_{52}O_{64}$ type of local order produces no better agreement with the observed patterns than does, *e.g.*, the f.c.c.-type arrangement; which, incidentally, involves only one of the two sets of tetrahedral positions and hence only one cluster orientation.

(*b*) *Partial Patterson projections*

These were calculated mainly in the ⟨311⟩-type projection, where all Bragg reflexions are of the type $(h+k+l=4n)$. One thus hoped to avoid serious Bragg scattering effects. The resulting map of projected order parameters [Fig. 8(*a*)] corresponds to the intensity distribution within the hatched area of Fig. 4(*c*), *minus* small regions around the Bragg spots. The same termination errors were included in the Patterson projections calculated from models [Fig. 8(*b*)–(*d*)]. The calculated values were given at intervals $\frac{1}{4}$[110] and $\frac{1}{44}$[332], which correspond to a net twice as dense as the projected interatomic vectors. There is, inevitably, considerable overlap of contributions from different vectors, both due to interatomic distances with different [113] components and because of termination errors. However, the inner region of the vector density map is seen to be consistent with a local arrangement of clusters.

(*c*) *The least-squares calculations*

These were all based upon the assumption of tetrahedral defect clusters. The intensity expression (8) was used and the order parameter associated with each shell of intercluster vectors was varied in order to obtain the best fit with the observed intensity distribution. Different numbers of intercluster vectors were tried, vectors less than the distance of closest approach being excluded. The order parameters given in Fig. 9 were obtained from [311] projection, the calculation included vectors up to [210]. In order to include more intensity data in the comparisons we used the order parameters from the [311] projection to calculate intensity distributions in other projections. Quite good qualitative agreement was then obtained, see Figs. 6 and 7(*a*) and (*f*). It should be noted that the agreement is considerably better than that obtained from domains of the ordered structure. The α's are normalized to the peak at the origin; this should be regarded as tentative, however, since the background subtraction procedure used allows no proper normalization.

Calculations based upon intensity expressions including Bragg scattering effects were also carried out, both in the form of least-squares calculations of order parameters and as intensity calculations from the order parameters which were obtained using kinematical expressions. The results in the projections [211], [311] and [411], which are the ones most extensively used in the present study, showed the Bragg scattering effects to be only moderate; they appear mainly as a redistribution of the diffuse scattering among Brillouin zones corresponding to the fundamental reflexions. In projections like [311], where the reflexions are of the type $h+k+l=4n$, these zones are identical with the Brillouin zones for the diffuse scattering. At the present level of accuracy, the results are therefore not felt to be seriously affected by Bragg scattering. The agreement between observed and calculated intensity in the [411] and [211] projections are improved slightly on introducing Bragg scattering. It appears, therefore, that these effects should be included if the accuracy is to be pursued further and especially if projections with stronger Bragg interactions are to be used.

Comparison between dynamical and kinematical intensity distributions for different Bragg conditions of the incident beam are shown in Fig. 10.

Discussion

Previous investigations of short-range-order scattering of electrons appear to have been concentrated upon qualitative features, like the shape of diffuse maxima,

Kohn-type anomalies or Fermi-surface effects (Castles, Cowley & Spargo, 1971; Watanabe & Fisher, 1967). Very recently, order parameters based upon the shape of the three-dimensional intensity distribution from $VC_{0.75}$ have been published by Sauvage & Parthé, 1972. The more quantitative crystallographic approach in terms of order parameters has thus largely been left to X-ray and neutron diffraction, leaving electron diffraction mainly as a method for qualitative survey of the intensity distribution.

The present study shows that calculations of order parameters may be pursued to some benefit even in electron diffraction, especially in cases like the one studied here, where the s.r.o. scattering features can be reasonably well separated from diffuse scattering from other sources. Our calculations are based largely upon kinematical scattering theory. The consideration of dynamical effects serves mainly as a guide to conditions where these can be minimized, but are also used to produce calculation methods which permit an estimation of the Bragg scattering effects. The choice of projections for which the Brillouin zones for diffuse scattering and for the fundamental reflexions are identical is a clear limitation, since the different positions involved in the ordering will then scatter in phase. This has, to a certain extent, been remedied in the present study through the comparisons made in other projections, *viz.* [411] and [211]. The possibility of exploiting the dynamical interactions to separate contribution from different sites to the s.r.o. scattering (Gjønnes & Høier, 1971) has yet to be explored in a systematic way. This would have to involve fairly dense projections

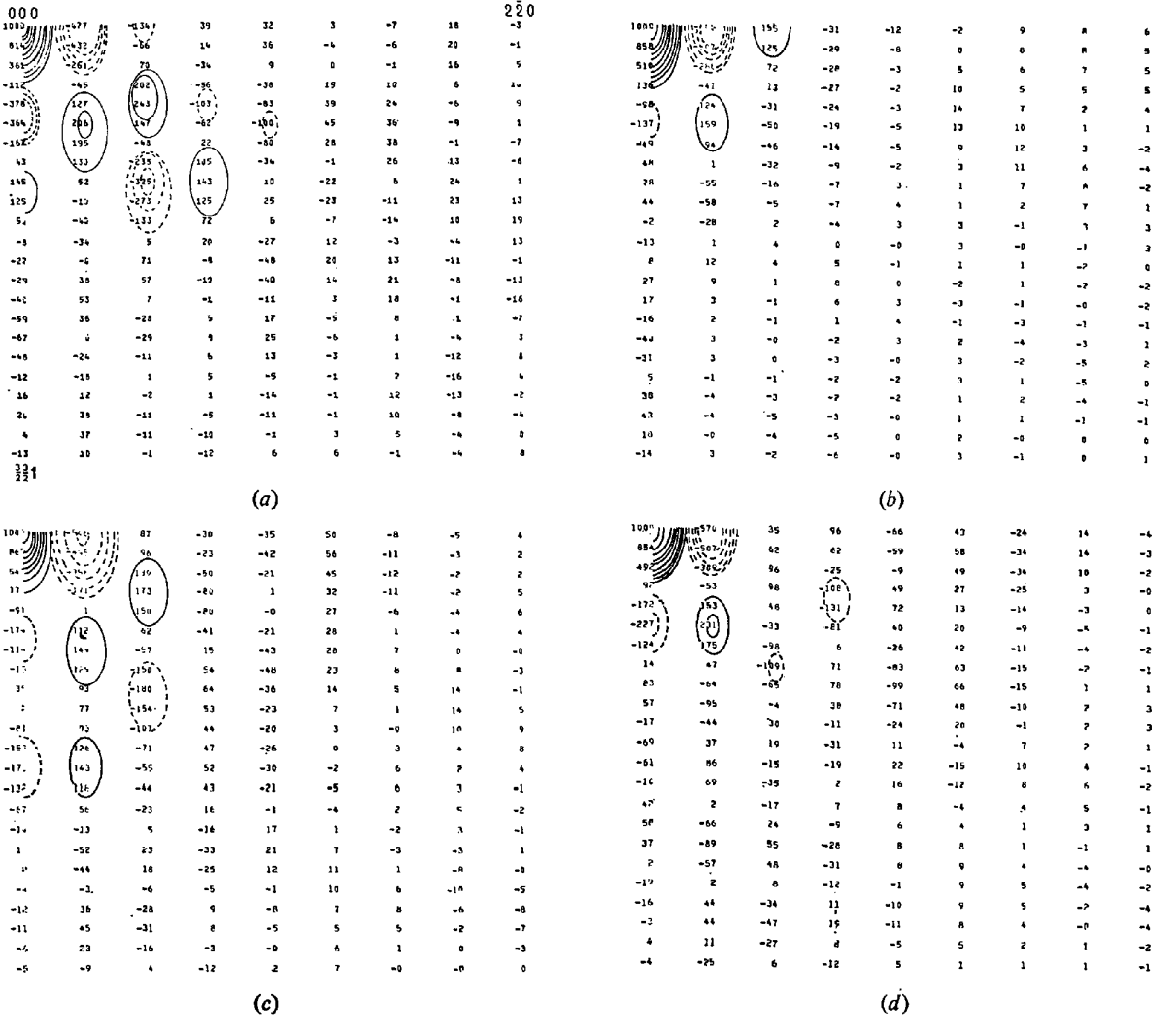

Fig. 8. The short-range parameters projected onto the (11$\bar{3}$) plane. (*a*) Calculated from the observed intensity distribution within the hatched area in Fig. 5(*c*). (*b*) Calculated from one cluster. (*c*) Calculated from one cluster at the origin and the probability 0·12 of having a cluster at $1\frac{1}{2}\frac{1}{2}$. (*d*) Calculated from one cluster at the origin and the probability 0·12 of having a cluster at $11\frac{1}{2}$.

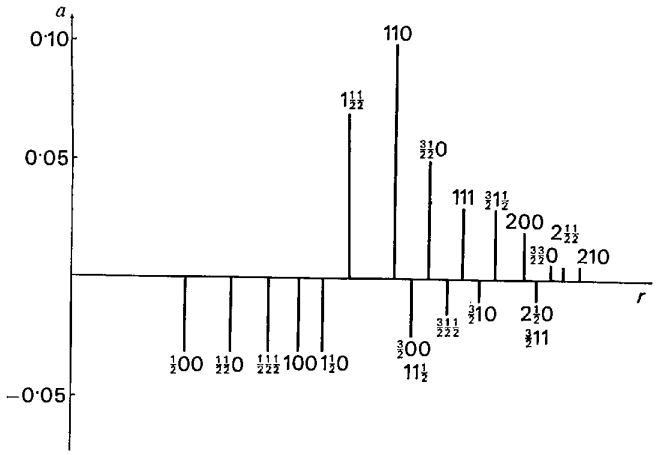

Fig. 9. Order parameters obtained from least-squares calculations in the (311) projection. These parameters were used for calculation of the distributions 6(*f*) and 7(*f*).

with reflexions of the types $h+k+l=4n+2$ and $h+k+l=4n\pm1$, *e.g.* [100], [110] or [310] for the present structure.

At the present stage the difficulties associated with the subtraction of a background appear to be more serious, however. These are partly to be attributed to uncertainties with regard to the shape and position of the smooth background, partly to the fact that the background should not be completely featureless, but include thermal scattering and Kikuchi line effects.

The latter effects can be calculated, at least approximately, and hence to a certain extent be corrected for; in the present study we have tried to minimize them through the choice of experimental conditions. If more reliable absolute values of order parameters are to be obtained, it will appear that the general shape of the featureless background should be studied in more detail. Such a study would definitely have to take multiple scattering into account, as was done by one of us

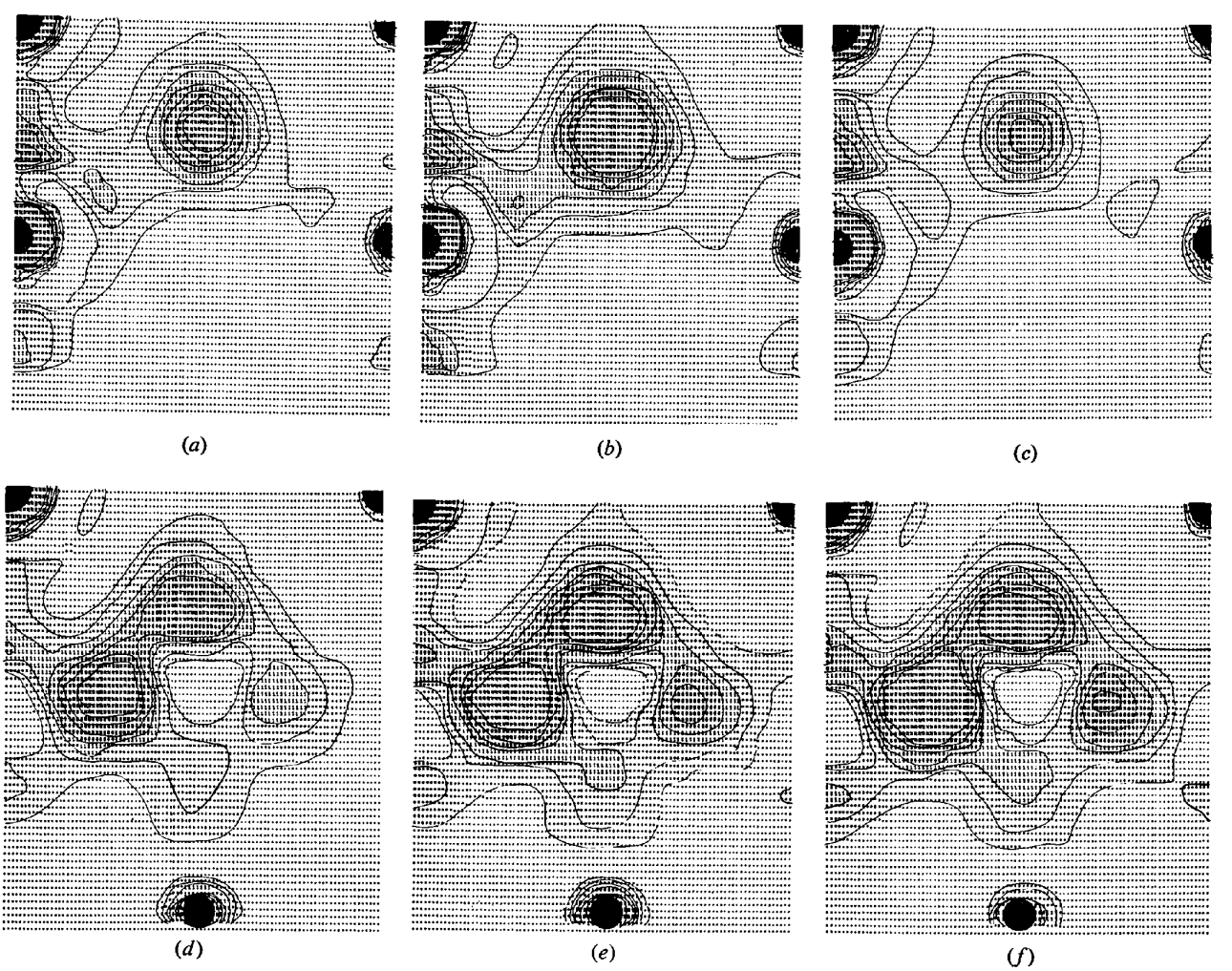

Fig. 10. Comparison between calculated kinematical and dynamical short-range-order scattering. (*a*) Kinematical (211) projection. (*b*) Dynamical (211) projection, symmetrical incidence. (*c*) Dynamical (211), 111 strongly excited ($s_{111}>0$). (*d*) Kinematical (411) projection. (*e*) Dynamical (411), symmetrical incidence. (*f*) Dynamical (411), 311 strongly excited.

some years ago in a study of scattering from thin amorphous films (Gjønnes, 1959). For a crystal such a multiple scattering calculation would have to include Kikuchi-line effects. Efforts in this direction have recently been made by Høier (1973). The exclusion of the inelastic part of the background through a velocity filter might reduce this problem considerably.

The question as to whether the comparison between observed and calculated distributions should be made in intensity space or in vector space is an old one in diffraction studies. With the quite complex structure studied in the present work, a least-squares method as employed has many advantages; it relates the intensity directly to a structure, and it does automatically take relations between different vectors in the projection into account. On the other hand, the use of the vector map may, to a certain extent, be seen as a more visual representation of the experimental results, and it does directly display some of the limitations inherent in the experiment, *e.g.* due to lack of observations close to the origin of the Brillouin zone.

The present investigation produces strong diffraction evidence for the existence of tetrahedral defect clusters in disordered $VO_{1.23}$. This was expected, since the ordered state can be considered as an ordered arrangement of such tetrahedra, and also because recent measurement of the 200 structure factor (Andersson & Høier, 1973) show that there must be nearly the same fraction of interstitial vanadium atoms above the ordering temperature.

The local arrangement of clusters in the disordered structure cannot as yet be described very precisely. The comparison between observed and calculated intensity distributions shows that the local arrangement deviates from the ordered structure, $V_{52}O_{64}$. The partial Patterson projection synthesis as well as the least-squares calculation of order parameters shows that $\langle 1\frac{1}{2}\frac{1}{2} \rangle$ is the nearest-neighbour intercluster vector. This is shorter than the nearest-neighbour vector $\langle 11\frac{1}{2} \rangle$ in the superstructure.

References

ANDERSSON, B. & GJØNNES, J. (1970). *Acta Chem. Scand.* **24**, 2250–2252.

ANDERSSON, B., GJØNNES, J. & TAFTØ, J. (1971). *Jernkont. Ann.* **155**, 457–458.

CASTLES, J. R., COWLEY, J. M. & SPARGO, A. E. C. (1971). *Acta Cryst.* A**27**, 376–383.

COWLEY, J. M. (1950). *J. Appl. Phys.* **21**, 24–30.

ELCOCK, E. W. (1956). *Order-Disorder Phenomena.* London: Methuen.

FISHER, P. (1965). *Int. Conf. on Electr. Diff. and Cryst. Defects, Melbourne,* IH-4. Melbourne: Australian Academy of Science.

GJØNNES, J. (1959). *Acta Cryst.* **12**, 976–980.

GJØNNES, J. (1965). *Int. Conf. on Electr. Diff. and Cryst. Defects, Melbourne,* IH-2. Melbourne: Australian Academy of Science.

GJØNNES, J. (1966). *Acta Cryst.* **20**, 240–249.

GJØNNES, J. & HØIER, R. (1971). *Acta Cryst.* A**27**, 166–174.

HØIER, R. (1973). *Acta Cryst.* A**29**, 663–672.

HØIER, R. & ANDERSSON, B. (1974). *Acta Cryst.* A **30**, 93–95.

SAUVAGE, M. & PARTHÉ, L. (1965). *Acta Cryst.* A**28**, 607–616.

WARREN, B. E., AVERBACH, B. L. & ROBERTS, B. W. (1951). *J. Appl. Phys.* **22**, 1493–1496.

WATANABE, D. & FISHER, P. (1965). *J. Phys. Soc. Japan.* **20**, 2170–2179.

WESTMAN, S. & NORDMARK, C. (1960). *Acta Chem. Scand.* **14**, 465–470.

Acta Cryst. (1974). A**30**, 224

Characterization of Twinning

BY A. SANTORO

Institute for Materials Research, National Bureau of Standards, Washington, D.C. 20234, *U.S.A.*

(*Received* 6 *August* 1973; *accepted* 26 *October* 1973)

A new twinning condition is derived. It is more general than Friedel's ratios [Friedel, G. (1964). *Leçons de Cristallographie*, p. 249, Paris: Blanchard], and it allows one to predict not only the twin laws of a crystalline species, but also the regular associations of crystals mutually oriented according to non-crystallographic rotations. The deviation suffered by the twin lattice at the composition surface is better described in terms of the new twinning condition than in terms of the twin obliquity.

Introduction

Assemblages of two or more crystals, of the same or of different species, are called *random aggregates* if the mutual orientation of the constituent crystals is haphazard, and *regular aggregates* or *oriented crystal growths* if the crystals are related in well-defined ways dictated by their lattice dimensions. The crystals of a regular aggregate are mutually oriented so that they have a row, a net or a lattice exactly or approximately in common. The lattice control dictating these three types of mutual orientations is called *monodimensional*, *didimensional* and *tridimensional* respectively. *Twins* are regular aggregates consisting of individual crystals of